ACS APPLIED NANO MATERIALS
Article
Cite This: ACS Appl. Nano Mater. 2019, 2, 6169−6177
www.acsanm.org

Photoelectrochemical Self-Powered Solar-Blind Photodetectors Based on Ga_2O_3 Nanorod Array/Electrolyte Solid/Liquid Heterojunctions with a Large Separation Interface of Photogenerated Carriers

Kai Chen,[†] Shunli Wang,[†] Chenran He,[†] Huiwen Zhu,[†] Hailin Zhao,[†] Daoyou Guo,[*,†,§] Zhengwei Chen,[‡] Jingqin Shen,[‡] Peigang Li,[*,‡] Aiping Liu,[†] Chaorong Li,[*,†] Fengmin Wu,[†] and Weihua Tang[‡]

[†]Center for Optoelectronics Materials and Devices & Key Laboratory of Optical Field Manipulation of Zhejiang Province, Department of Physics, Zhejiang Sci-Tech University, Hangzhou 310018, China

[‡]State Key Laboratory of Information Photonics and Optical Communications & Information Functional Materials and Devices, School of Science, Beijing University of Posts and Telecommunications, Beijing 100876, China

[§]State Key Lab of Silicon Materials, Zhejiang University, Hangzhou 310027, China

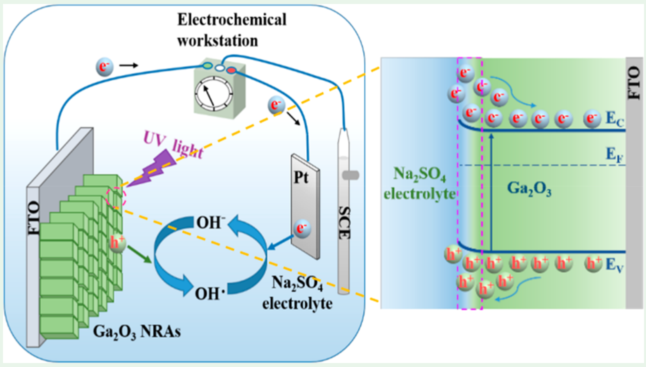

ABSTRACT: Solar-blind photodetectors have been widely developed because of their great potential application in biological analysis, ultraviolet communication, and so on. Photodetectors constructed by vertically aligned nanorod arrays (NRAs), have attracted intensive interest recently owing to the virtues of low light reflectivity and rapid electron transport. However, limited by the insufficient contact between the upper electrode and NRAs because of uneven NRAs, photogenerated carriers cannot be effectively separated and transferred. In this work, a novel photoelectrochemical (PEC) type self-powered solar-blind photodetectors constructed in the form of Ga_2O_3 NRAs/electrolyte solid/liquid heterojunction with a large photogenerated carrier separation interface has been fabricated, β-Ga_2O_3 NRAs PEC photodetector shows a photoresponsivity of 3.81 mA/W at a bias voltage of 0 V under the 254 nm light illumination with the light intensity of 2.8 mW/cm^2, thus yielding a I_{photo}/I_{dark} ratio of 28.97 and an external quantum efficiency of 1.86%. Our results provide a novel device structure of solar-blind photodetector with high efficient deep-ultraviolet photodetection and low power consumption.

KEYWORDS: *Ga_2O_3 NRAs, solar-blind photodetectors, self-powered, photoelectrochemical, solid−liquid heterojunction*

1. INTRODUCTION

Solar-blind photodetectors have attracted vast attention because of their all-weather operation environment and accurate detection rate in biological analysis, environmental monitoring, ultraviolet communication, solar-blind imaging, and many other fields.[1−4] To date, various ultrawide band gap semiconductors such as AlGaN,[5] ZnMgO,[6] diamond,[7] Ga_2O_3,[8,9] etc., have been employed to fabricate solar-blind photodetectors. Among these materials, Ga_2O_3 is a natural choice for use in solar-blind photodetectors[10−12] due to the virtues of direct bandgap of ∼4.9 eV which is in the solar-blind region. It could be directly used with the necessity to tune the band gap in avoiding phase separation and alloy composition fluctuations.[5,6,8−12]

A modern solar-blind photodetectors with low energy consumption and 5S (high sensitivity, high spectral selectivity, high signal-to-noise ratio, high speed, high stability) are pursued by researchers.[2,13−19] Various nanostructures materials such as nanoparticles,[20,21] nanowires,[22,23] films,[9,24,25] and aligned nanorod arrays (NRAs)[26−28] have been used to construct the photosensitive layers for solar-blind photodetectors. The one-dimensional vertical NRAs is in particular preferred thanks to its massive surface-to-volume ratio, low light reflectivity and efficient coupling with incident light, which can provide a fast channel for the photogenerated carriers transport.[29] Recently, the graphene/vertical Ga_2O_3 nanowire array heterojunction for the solar-blind deep-ultraviolet photodetection has been fabricated.[30] However, the photogenerated carriers can not be separated and transferred effectively because the graphene electrode only contacts with part of the upper end of the nanorods due to uneven NRAs. Compared with those conventional photo-

Received: May 25, 2019
Accepted: September 13, 2019
Published: September 13, 2019

DOI: 10.1021/acsanm.9b00992
ACS Appl. Nano Mater. 2019, 2, 6169−6177

Scheme 1. Schematic Illustration of the Fabrication Process of Ga_2O_3 NRAs

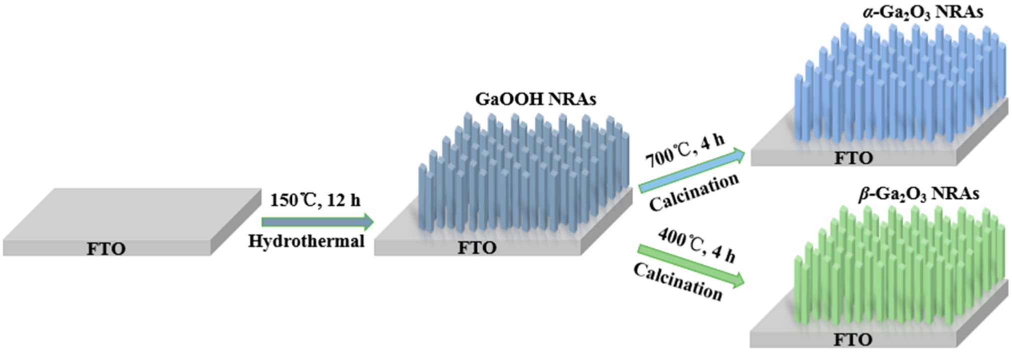

detectors which must be powered by an external power source, self-powered photodetectors can work without an external power supply and meet the requirements of lightweight, small size, and low power consumption. It has been demonstrated that the self-powered photodetector can be realized by using the *p-n* junction,[31−33] Schottky junction,[34,35] heterojunction,[36] and photoelectrochemical (PEC) cell.[37,38] Among them, the Ga_2O_3-based self-powered solar-blind photodetector belonging to family of PEC devices exhibits great promise in due to its large contact area of solid/liquid interface and low-cost, simple manufacturing process.

In this paper, α and β phases Ga_2O_3 vertically aligned NRAs were synthesized by a combined hydrothermal and post-annealed method. A novel PEC self-powered solar-blind photodetector was then assembled by separately using the α and β phases of Ga_2O_3 NRAs as the active photoanodes. The β-Ga_2O_3 NRAs-based device shows a higher photosensitivity and a faster photoresponse time than the α-Ga_2O_3 NRAs-based device. This work provides a novel device structure of solar-blind photodetector with high efficient deep-ultraviolet photodetection and low power consumption.

2. EXPERIMENTAL DETAILS

2.1. Material Synthesis. The details of GaOOH NRAs synthesis were described in previous work.[15] The α-Ga_2O_3 and β-Ga_2O_3 NRAs were obtained by annealing GaOOH NRAs at 400 and 700 °C, respectively, in atmospheric environment for 4 h. The schematic illustration of the Ga_2O_3 NRAs synthesis is shown in Scheme 1.

2.2. Materials Characterization. The morphologies were characterized on a field-emission scanning electron microscope (FESEM) and a transmission electron microscope. (TEM). The crystalline structure was examined on a X-ray diffractometer (XRD) and ultraviolet−visible (UV−vis) absorption spectra. The surface compositions checked on a X-ray photoelectron spectroscopy (XPS) can be referred to in our previous work.[15] The Raman spectra were measured on a LabRam HR high resolution spectrometer equipped with a microscope. Fourier-transform infrared (FTIR) spectra were measured on a Nicolet 5700 FT-IR spectrometer. Photoluminescence (PL) spectra were recorded with an excitation wavelength of 266 nm.

2.3. Device Measurements. The electrical characterization was carried out in a three-electrode configuration on a CHI 760E electrochemical workstation (Chenhua Instrument Company, China). The Ga_2O_3 NRAs grown on FTO substrate was used as the working electrode, platinum foil (10×15 mm^2) as counter electrode and saturated calomel electrode (SCE) as reference electrode. A 254 nm UV lamp with a power of 7 W was used as the illumination source. A 0.5 M Na_2SO_4 aqueous solution was used as the electrolyte. The active area of Ga_2O_3 NRAs/FTO photoanode was fixed at 1 cm^2. The Mott−Schottky (M-S) plots and electrochemical impedance spectroscopy (EIS) measurements were carried out at 1.0 kHz in dark.

3. RESULTS AND DISCUSSION

3.1. Morphology and Crystal Structure of Ga_2O_3 NRAs. The top-view and cross-sectional FESEM of as-grown α-Ga_2O_3 NRAs are shown in Figure 1(a) and (b), respectively. The nanorod has an average length of 1.49 μm and a diameter ranging from 100 to 500 nm. The tips of nanorods are diamond-shaped and has not been affected by the postannealing seen from the top-view FESEM of α-Ga_2O_3 and β-Ga_2O_3 NRAs, as shown in Figure 1(c) and (d), respectively. As is shown in the inset of Figure 1(d), the spacing between two adjacent lattice fringes was calculated to be 0.288 nm, which corresponds to that of the β-Ga_2O_3 (002) plane, confirming formation of the monoclinic structure.[38,39]

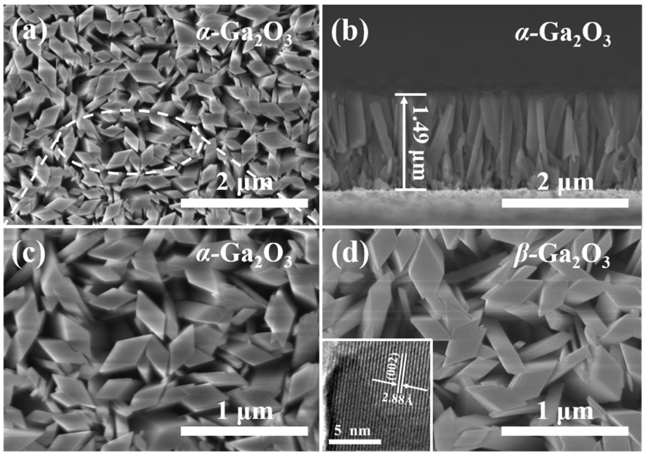

Figure 1. Top viewsof FESEM images at low (a) and high (c) magnification of α-Ga_2O_3 NRAs grown on the FTO substrate. (b) Cross-sectional FESEM image of α-Ga_2O_3 NRAs. (d) The top view of β-Ga_2O_3 NRAs at high magnification. The inset shows HR-TEM image of β-Ga_2O_3 nanorod.

Figure 2(a) shows the typical XRD patterns of the FTO/GaOOH, FTO/α-Ga_2O_3 and FTO/β-Ga_2O_3, respectively. Impurity SnO_2 peak, which is arisen from the FTO substrate, is observed. Besides the peaks from FTO/GaOOH, two peaks located at 36.0°, 64.7° were observed in FTO/α-Ga_2O_3, which correspond to the (110) and (300) planes of α-Ga_2O_3 with a trigonal structure (JCPDS file No.06−0180). The α-Ga_2O_3NRAs show a preferred growth orientation perpendicular to (110) plane. Three diffraction peaks arising from the (002), (111), and (401) planes of β-Ga_2O_3 with a monoclinic structure (JCPDS file No.43−1012) were found at 31.7°, 35.3°, and 37.9°.[38,39] The sharp and intense diffraction peak of

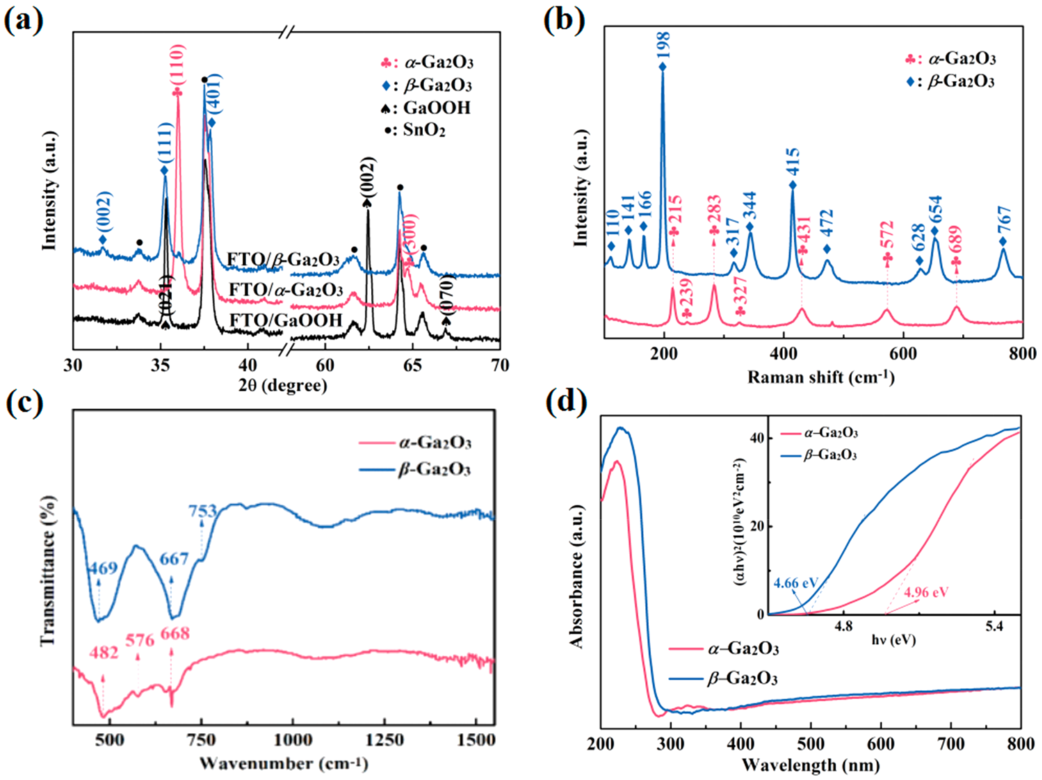

Figure 2. (a) XRD patterns of the FTO/GaOOH NRAs, FTO/α-Ga_2O_3 NRAs, and FTO/β-Ga_2O_3 NRAs. (b) Raman and (c) FTIR spectra of α-Ga_2O_3 and β-Ga_2O_3 nanorods. (d) The absorption spectra of α-Ga_2O_3 and β-Ga_2O_3 nanorods, insert is the plot of $(\alpha h\nu)^2$ versus the light energy ($h\nu$).

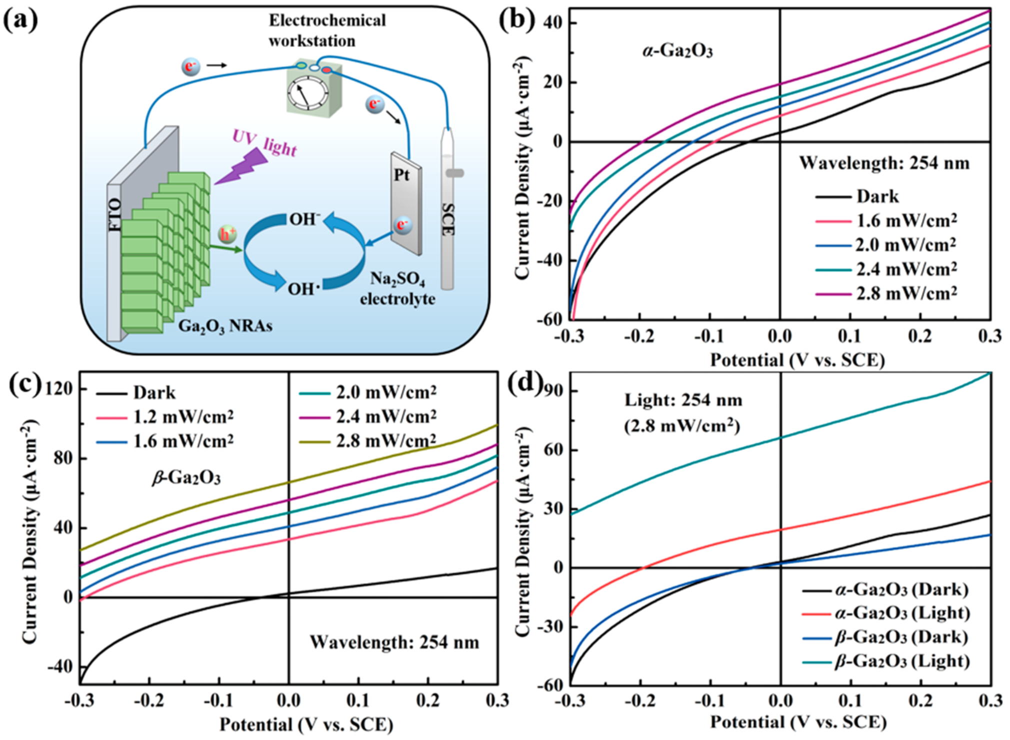

Figure 3. (a) Structural diagram of Ga_2O_3 NRAs PEC photodetectors. LSV curves of (b) α-Ga_2O_3 and (c) β-Ga_2O_3 NRAs PEC photodetector in dark and under the 254 nm light illumination with various light intensities. (d) The LSV curves of α-Ga_2O_3 and β-Ga_2O_3 NRAs photodetector are compared under the same conditions.

the (111) plane indicates that the β-Ga_2O_3 NRAs are grown along the (111) crystal plane. The XRD result indicates that GaOOH was converted to crystalline α-Ga_2O_3 or β-Ga_2O_3 during the post annealing process.

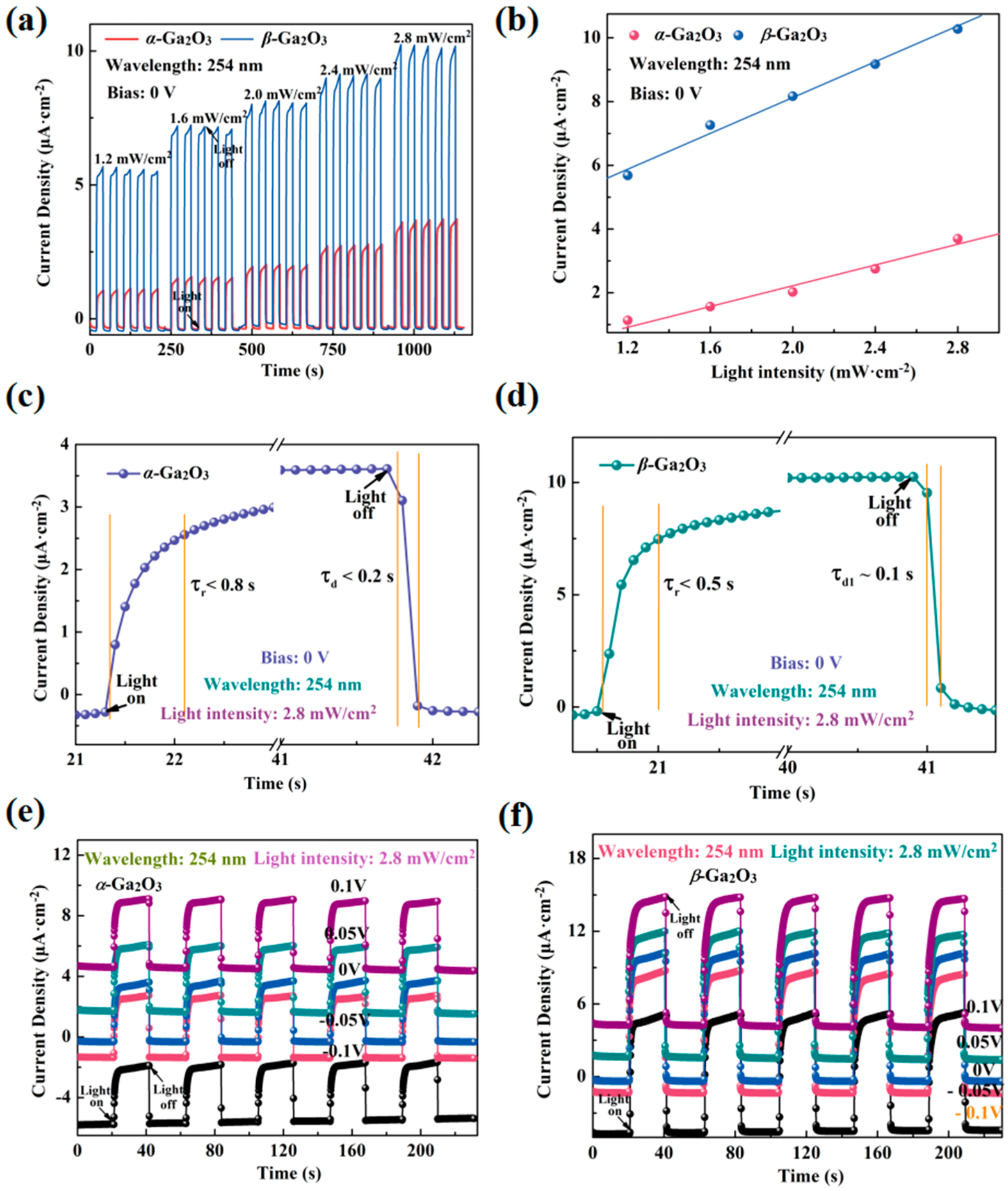

Figure 4. (a) I-t curves of the Ga_2O_3 NRAs PEC photodetectors for the 254 nm light illumination with various light intensities at 0 V vs SCE. (b) The relationship between the light intensity and photocurrent. Rise time and decay time of (c) α-Ga_2O_3 and (d) β-Ga_2O_3 NRAs PEC photodetectors at 0 V vs SCE under the 254 nm light illumination with the light intensity of 2.8 mW/cm^2. Photoresponse switching behaviors of (e) α-Ga_2O_3 and (f) β-Ga_2O_3 NRAs PEC photodetectors at various applied bias.

The trigonal α-Ga_2O_3 with the spapce group of the R_{3c} symmetry consists of GaO_6 octahedra. While monoclinic β-Ga_2O_3 in the C_{2h} space group contains of both GaO_6 octahedra and GaO_4 tetrahedra.[40] The Raman spectra of the α-Ga_2O_3 and β-Ga_2O_3 nanorods are shown in Figure 2(b). Seven frequencies of 215, 239, 283, 327, 431, 572, and 689 cm^{-1} are detected for the sample annealed at 400 °C, which could be assigned to α-Ga_2O_3.[41] While for the sample annealed at 700 °C, 11 active modes at 110, 141, 166, 198, 317, 344, 415, 472, 628, 654, and 767 cm^{-1} appeared, corresponding to the characteristic peaks of β-Ga_2O_3.[40] The strong peaks centered at 667 and 753 cm^{-1} of FTIR spectra in Figure 2(c) are attributed to the contraction vibrations of Ga−O bonds in the lattice formed by the GaO_6 octahedra and the regular GaO_4 tetrahedra of β-Ga_2O_3 nanorods, respectively.[42,43] While a broad band peak of α-Ga_2O_3 nanorods centered at 668 cm^{-1} resulted from the Ga−O vibrations of GaO_6 octahedra.[44,45] These results of Raman and FTIR spectra consistent with the XRD results indicate the formation of α- and β-Ga_2O_3 when annealed the sample at 400 and 700 °C, respectively.

The band gaps of α-Ga_2O_3 and β-Ga_2O_3 are calculated from the UV−vis absorbance spectra presented in Figure 2(d) and its inset. The absorption edge of β-Ga_2O_3 is at ∼266 nm and that of α-Ga_2O_3 exhibits a blue shift. The band gaps of α-Ga_2O_3 and β-Ga_2O_3 are ∼4.96 and 4.66 eV respectively estimated from the curves of $(\alpha h\nu)^2$ versus $h\nu$. Both of them are capable of absorbing the deep ultraviolet light, which are promising candidate materials for solar-blind photodetection.

3.2. Photoelectric Characteristic of Ga_2O_3 NRAs PEC Solar-Blind Photodetectors. The schematic illustration for measuring the photoelectric properties of the Ga_2O_3 NRAs PEC photodetectors by using the three-electrode system is presented in Figure 3(a). The typical linear sweep voltammetry (LSV) curves of α-Ga_2O_3 and β-Ga_2O_3NRAs photodetectors

DOI: 10.1021/acsanm.9b00992
ACS Appl. Nano Mater. 2019, 2, 6169−6177

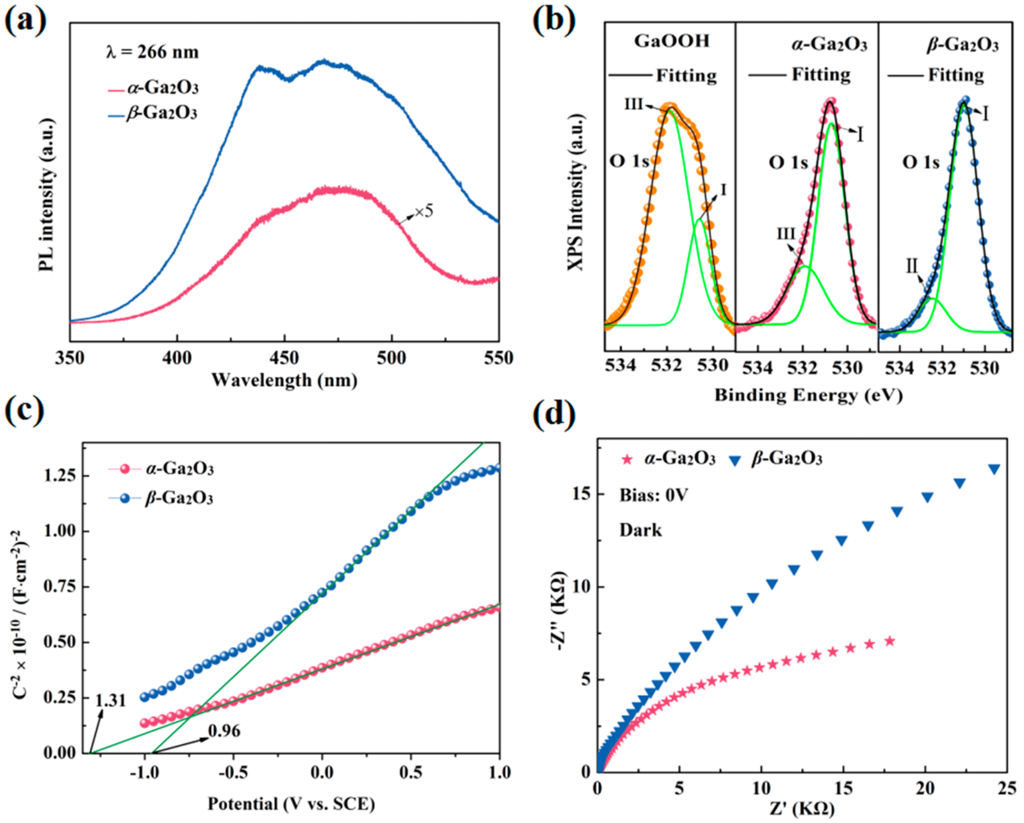

Figure 5. (a) The PL spectra of the α-Ga_2O_3 and β-Ga_2O_3 nanorods excited by 266 nm laser. (b) XPS spectra of O 1s core levels in GaOOH, α-Ga_2O_3 NRAs and β-Ga_2O_3 NRAs respectively. (b) M−S plots of α-Ga_2O_3 and β-Ga_2O_3 NRAs were measured at a frequency of 1.0 kHz in an aqueous solution of 0.5 M Na_2SO_4. (c) The EIS plots of α-Ga_2O_3 and β-Ga_2O_3 NRAs were measured from 100 kHz to 0.01 Hz at 0 V vs SCE in dark.

are visible in Figure 3(b) and (c), respectively. Dark current densities show typical rectification characteristics, which can be attributed to the energy band bending of Ga_2O_3 NRAs at the interface of solid/liquid. With the increase of the light intensity from 1.6 to 2.8 mW/cm^2, the photocurrent density of α-Ga_2O_3 NRAs photodetector was increased gradually from 8.80 to 19.49 μA/cm^2 under the bias of 0 V. While for the β-Ga_2O_3 NRAs photodetector, the photocurrent density could be increased from 41.14 to 66.34 μA/cm^2. The above experimental results demonstrated that the device can work without external power supply. Seeing from the LSV curves in Figure 3(d), the dark current densities of α-Ga_2O_3 and β-Ga_2O_3 NRAs photodetectors are approximately 3.15 μA/cm^2 and 2.29 μA/cm^2 at 0 V, respectively. The light/dark ratio (I_{light}/I_{dark}) of β-Ga_2O_3 NRAs photodetector is 28.97 under the254 nm light illumination with the light intensity of 2.8 mW/cm^2, which is about 4.7 times the value of α-Ga_2O_3. The above results demonstrated that the β-Ga_2O_3 NRAs photodetector is more photosensitive to solar-blind deep-ultraviolet light than the α-Ga_2O_3 devices.

The time-resolved photoresponse was performed under the illumination of 254 nm light by a switching on/off interval of 20 s at 0 V, as displayed in Figure 4(a). Both the α-Ga_2O_3 and β-Ga_2O_3 NRAs PEC photodetectors perform stably and reproducibly. Meanwhile, the photocurrent increases linearly with the increase of the light intensity, seen in Figure 4(b). The Ga_2O_3 NRAs PEC photodetectors exhibit a maximal photocurrent under the 254 nm light irradiation with the incident light intensity of 2.8 mW/cm^2. The calculated photoresponsivity (R_λ) and external quantum efficiency (EQE) are 1.44 mA/W and 0.70% for the α-Ga_2O_3 NRAs PEC photodetectors, respectively.[46,47] Whereas for the β-Ga_2O_3 devices, R_λ and EQE are 3.81 mA/W and 1.86%, respectively.

Figure 4(c) and (d) enlarge the view of the rising and decaying edges of the photoresponse to the 2.8 mW/cm^2 254 nm light irradiation at 0 V. The rise time ($\boldsymbol{\tau}_r$) is defined as the time required for the current rising from 10% to 90% of the maximum, and the decay time ($\boldsymbol{\tau}_d$) is the time taken by the photocurrent decreasing from 90% of the maximum to 10%.[48] The $\boldsymbol{\tau}_r$ of α-Ga_2O_3 and β-Ga_2O_3 NRAs PEC photodetectors are shorter than 0.5 s and 0.3, s respectively, and both of the $\boldsymbol{\tau}_d$ are less than 0.2 s.

Meanwhile, the photoelectric performance of the PEC photodetectors can be apparently improved by the applied bias. The photoresponse curves of α-Ga_2O_3 and β-Ga_2O_3 NRAs PEC photodetectors under various applied bias were obtained, seen in Figure 4(e) and (f). When the applied bias was increased from −0.1 to 0.1 V, both the dark current and photocurrent were clearly increased. For the β-Ga_2O_3 photodetector, the photocurrent is 14.82 μA/cm^2 at 0.1 V, which is 2.87 times the value of that at −0.1 V. The improved photocurrent by the external bias potential can be attributed to the more effective separation of electron−hole pairs.

3.3. The Working Mechanism Analysis of Ga_2O_3 NRAs PEC Photodetectors. The room-temperature PL spectra of the α-Ga_2O_3 and β-Ga_2O_3 nanorods excited by 266 nm laser are depicted in Figure 5(a). Both of them show a broad visible

Table 1. Comparison of the Photoelectric Performance of the Ga_2O_3NRAs PEC Photodetectors in This Work and the PEC Self-Powered Photodetectors Reported by Others

photoelectrode	condition	electrolyte type	electrode system	rise time (s)	decay time (s)	I_{light}/I_{dark} ratios	photoresponsivity (mA/W)	efficiency (%)	reference
ZnO NRs	250−600 nm (100 mW/cm^2), 0 V	Na_2SO_4	3-electrode	4.9	134.3	7			54
TiO_2 NRAs	365 nm (3 mW/cm^2), 0 V	Na_2SO_4	3-electrode	<0.1	<0.1	6	5		55
ZnO NAs/G/Cu_2O	365 nm (0.5 mW/cm^2), 0 V	Na_2SO_4	3-electrode	0.006	0.006	3.5	21.2		56
ZnO NRs	385 nm (1.25 mW/cm^2), 0 V	water	2-electrode	0.1	0.1		22		57
TiO_2 NRAs	365 nm (1.25 mW/cm^2), 0 V	water	2-electrode	0.15	0.05		25 at 350 nm		58
α-Ga_2O_3 NRAs	254 nm (0.4 mW/cm^2), 0 V	NaOH	2-electrode	0.076	0.056		0.21		59
α-Ga_2O_3 NRAs	254 nm (2.8 mW/cm^2), 0 V	Na_2SO_4	3-electrode	0.43	0.17	6.19	1.44	0.70	this work
β-Ga_2O_3 NRAs	254 nm (2.8 mW/cm^2), 0 V	Na_2SO_4	3-electrode	0.29	0.16	28.97	3.81	1.86	

emission band from 380 to 550 nm, which is usually attributed to oxygen vacancies.[49] It can be observed that the PL intensity of β-Ga_2O_3 nanorods is much stronger than that of α-Ga_2O_3 due to the more oxygen vacancies.

Figure 5(b) shows the O 1s core level peaks of the GaOOH, α-Ga_2O_3 and β-Ga_2O_3 NRAs, which can be marked as peak I, II, and III. The peak I centered at about 530.7 eV is arisen from the O 1s core level in the Ga_2O_3, the peak IIat 532.5 eV is associated with defect sites with a low oxygen coordination such as oxygen vacancies, while the peak III at 531.9 eV is associated with surface adsorbed or chemisorbed hydroxy species. The main peak of III can be found in GaOOH due to the hydroxyl, while the main peak of both α-Ga_2O_3 and β-Ga_2O_3 NRAs is I because of Ga−O bonding. The stronger peak of III in α-Ga_2O_3 is due to that there are many hydroxy species adsorbed or chemisorbed at the surface with a lower temperature annealing, while the stronger peak of II in β-Ga_2O_3 is caused by the more oxygen vacancies. The result of XPS is consistent with that of PL.

To further understand the conductivity and the charge transport properties of the Ga_2O_3 NRAs, *M*−*S* plots were obtained in a 0.5 M Na_2SO_4 aqueous solution, seen in Figure 5(c). The capacitance of the space charge region between semiconductor and electrolyte can be quantified by the *M*−*S* equation:[50,51]

$$1/C^2 = (2/e\varepsilon\varepsilon_0 N_D)[(V - V_{FB}) - kT/e] \tag{1}$$

where C is the capacitance of the space charge layer, ε represents the relative permittivity of the semiconductor (ε of Ga_2O_3 is 10), and e, ε_0, k, V, and T represent the electron charge, the vacuum permittivity, the Boltzmann constant, the applied potential, and the absolute temperature, respectively. The kT/e item is often neglected because of the extremely small value. The flat band potential (V_{FB}) can be estimated through an extrapolation of the *M*−*S* plots. The concentration of donors (N_D) can be calculated from the slope of the *MS* plots using the following equation:[52,53]

$$N_D = (2/e\varepsilon\varepsilon_0)[d(1/C^2)/dV]^{-1} \tag{2}$$

The positive slope of the plots indicates that Ga_2O_3 is an *n*-type semiconductor. The estimated V_{FB} of α-Ga_2O_3 and β-Ga_2O_3 are −1.31 V and −0.96 V (vs. SCE), respectively. The corresponding N_D of α-Ga_2O_3 and β-Ga_2O_3 are 4.88×10^{19} cm^{-3}, 1.97×10^{19} cm^{-3}, respectively. The larger carrier concentration in α-Ga_2O_3 NRAs leads to a larger dark current of the α-Ga_2O_3 photodetector than that of the β-Ga_2O_3 device.

Figure 5(d) shows the EIS plots of the α-Ga_2O_3 and β-Ga_2O_3 NRAs measured at 0 V vs. SCE in dark. The α-Ga_2O_3 NRAs PEC photodetector has a smaller radius than that of the β-Ga_2O_3 device, indicating that the faster transport of electrons at the interface of α-Ga_2O_3 NRAs/electrolyte. The result is consistent with the those derived from the LSV and *M*−*S* measurements.

Table 1 lists the parameters of the Ga_2O_3NRAs PEC photodetectors in this work and those of the PEC self-powered photodetectors reported by others.[54−59] Most of the previously reported PEC self-powered photodetectors are constructed by using the wide bandgap semiconductor materials, such as ZnO and TiO_2, which are photosensitive to the ultraviolet illumination, for example, by using the light with the wavelength of 365 nm.[54−58] The I_{light}/I_{dark} ratio of our PEC photodetector based on β-Ga_2O_3 NRAs is larger than those previously reported, though other parameters are comparable. Recently, Zhang et al. reported a self-powered solar-blind PEC photodetector based on α-Ga_2O_3 NRAs, which shows a fast photoresponse to the UV light of 254 nm with a rise time of 0.076 s and decay time of 0.056 s.[59] However, the photoresponsivity of their device is only 0.21 mA/W. Our β-Ga_2O_3NRAs PEC photodetector shows a photoresponsivity of 3.81 mA/W at 0 V under the illumination of 254 nm light, which is 18 times larger than their value. Although the α-Ga_2O_3 NRAs PEC photodetector exhibits a poorer photoelectric performance than the β-Ga_2O_3 device in our study, the photoresponsivity is also nearly 7 times larger than the value reported in ref 59.

Figure 6 illustrates the energy band diagram of the Ga_2O_3 NRAs PEC photodetectors. The redox potential of the electrolyte of Na_2SO_4 aqueous is lower than the Fermi level of the *n*-type Ga_2O_3 NRAs. When they contacts with each other, the space charge layer will form because of the charge distribution difference between the materials. A built-in electric field will then be generated between the Ga_2O_3 NRAs and Na_2SO_4 aqueous. When deep-ultraviolet light irraditate the Ga_2O_3 NRAs PEC photodetectors, the electrons of the valence band (VB) will be excited to the conduction band (CB), thus leaving the holes in the VB. The photogenerated holes in the VB of Ga_2O_3 will then gather at the interface of Ga_2O_3/electrolyte and capture the OH^- anions from the Na_2SO_4

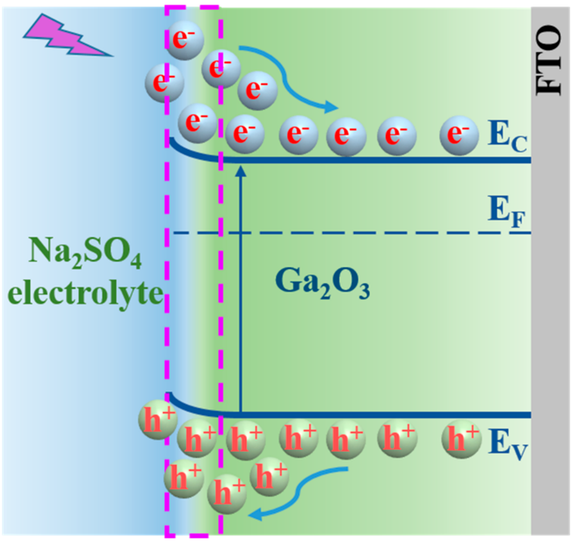

Figure 6. A schematic of the energy band at the Ga_2O_3 NRAs/electrolyte interface.

aqueous ($h^+ + OH^- \rightarrow OH\cdot$), as shown in Figure 3(a). Meanwhile, the photogenerated electrons will transport onto the CB of Ga_2O_3 and then are collected by FTO substrate directly. The photogenerated electrons reduce radical OH· to the OH^- anions at the Pt/electrolyte interface ($OH\cdot + e^- \rightarrow OH^-$).

4. CONCLUSIONS

To solve the inadequate contact problem between the upper electrode and NRAs, the PEC self-powered solar-blind photodetectors with a large separation interface of photogenerated carriers were assembled by using the α-Ga_2O_3 or β-Ga_2O_3 NRAs as the active photoanode. The β-Ga_2O_3 NRAs PEC self-powered solar-blind photodetector shows a better photoelectric performance than that constructed by using the α-Ga_2O_3 device. Under 254 nm light illumination with the light intensity of 2.8 mW/cm^2, a R_λ of 3.81 mA/W, a I_{light}/I_{dark} ratio of 28.97, and a photoresponse decay time less than 0.2 s, are obtained for the β-Ga_2O_3 NRAs/electrolyte solid−liquid heterojunction photodetector. These PEC self-powered solar-blind photodetectors based on Ga_2O_3 NRAs/electrolyte solid−liquid heterojunction with highly efficient electrons collection and low power consumption, are promising candidates for the future solar-blind photodetection.

■ AUTHOR INFORMATION

Corresponding Authors

*(D.Y.G.) E-mail: dyguo@zstu.edu.cn.
*(P.G.L.) E-mail: pgli@bupt.edu.cn.
*(C.R.L.) E-mail: crli@zstu.edu.cn.

ORCID

Daoyou Guo: 0000-0002-6191-1655
Aiping Liu: 0000-0002-2338-062X

Notes

The authors declare no competing financial interest.

■ ACKNOWLEDGMENTS

This work was supported by the National Natural Science Foundation of China (Nos 61704153, 51572241, 61774019, 51572033), Zhejiang Public Service Technology Research Program/Analytical Test (LGC19F040001), Beijing Municipal Commission of Science and Technology (SX2018-04), Visiting Scholar Foundation of State Key Lab of Silicon Materials (SKL2019-08), Fundamental Research Funds of Zhejiang Sci-Tech University (2019Q061, 2019Q066), Science Foundation of Zhejiang Sci-Tech University (ZSTU) (No. 0913850-Y), and the Open Fundof IPOC (BUPT). We thank to Dr. Yanfeng Guo from Shanghai Tech University for polishing the English.

■ REFERENCES

(1) Shepelev, V. A.; Altukhov, A. A.; Gladchenkov, E. V.; Popov, A. V.; Teplova, T. B.; Feshchenko, V. S.; Zhukov, A. O. Measuring the Optical Density of Wastewater by means of a Diamond UV Photodetector. *Russ. Eng. Res.* **2017**, *37* (3), 273−275.

(2) Guo, D. Y.; Liu, H.; Li, P. G.; Wu, Z. P.; Wang, S. L.; Cui, C.; Li, C. R.; Tang, W. H. Zero-Power-Consumption Solar-Blind Photodetector Based on β-Ga_2O_3/NSTO Heterojunction. *ACS Appl. Mater. Interfaces* **2017**, *9* (2), 1619−1628.

(3) Lin, C. N.; Lu, Y. J.; Yang, X.; Tian, Y. Z.; Gao, C. J.; Sun, J. L.; Dong, L.; Zhong, F.; Hu, W. D.; Shan, C. X. Diamond-Based All-Carbon Photodetectors for Solar-Blind Imaging. *Adv. Opt. Mater.* **2018**, *6* (15), 1800068.

(4) Zhuo, R.; Wang, Y.; Wu, D.; Lou, Z.; Shi, Z.; Xu, T.; Xu, J.; Tian, Y.; Li, X. High-performance Self-Powered Deep Ultraviolet Photodetector Based on MoS_2/GaN *p-n* Heterojunction. *J. Mater. Chem. C* **2018**, *6* (2), 299−303.

(5) Cho, C. Y.; Zhang, Y.; Cicek, E.; Rahnema, B.; Bai, Y.; McClintock, R.; Razeghi, M. Surface Plasmon Enhanced Light Emission from AlGaN-based Ultraviolet Light-Emitting Diodes Grown on Si (111). *Appl. Phys. Lett.* **2013**, *102* (21), 211110.

(6) Teherani, F. H.; Look, D. C.; Rogers, D. J.; Hierro, A.; Tabares, G.; Lopez-Ponce, M.; Ulloa, J. M.; Kurtz, A.; Munoz, E.; Marín-Borras, V.; Munoz-Sanjose, V.; Chauveau, J. M. ZnMgO-Based UV Photodiodes: A Comparison of Films Grown by Spray Pyrolysis and MBE. *Proc. SPIE* **2016**, *9749*, 1−4.

(7) Liu, Z.; Zhao, D.; Ao, J. P.; Wang, W.; Chang, X.; Wang, Y.; Fu, J.; Wang, H. X. Enhanced Ultraviolet Photoresponse of Diamond Photodetector Using Patterned Diamond Film and Two-Step Growth Process. *Mater. Sci. Semicond. Process.* **2019**, *89*, 110−115.

(8) Guo, D. Y.; Wu, Z. P.; Li, P. G.; An, Y. H.; Liu, H.; Guo, X. C.; Yan, H.; Wang, G. F.; Sun, C. L.; Li, L. H.; Tang, W. H. Fabrication of β-Ga_2O_3 Thin Films and Solar-Blind Photodetectors by Laser MBE Technology. *Opt. Mater. Express* **2014**, *4* (5), 1067.

(9) Guo, D. Y.; Wu, Z. P.; An, Y. H.; Guo, X. C.; Chu, X. L.; Sun, C. L.; Li, L. H.; Li, P. G.; Tang, W. H. Oxygen Vacancy Tuned Ohmic-Schottky Conversion for Enhanced Performance in β-Ga_2O_3 Solar-Blind Ultraviolet Photodetectors. *Appl. Phys. Lett.* **2014**, *105* (2), 023507.

(10) Guo, D. Y.; Shi, H. Z.; Qian, Y. P.; Lv, M.; Li, P. G.; Su, Y. L.; Liu, Q.; Chen, K.; Wang, S. L.; Cui, C.; Li, C. R.; Tang, W. H. Fabrication ofβ-Ga_2O_3/ZnO Heterojunction for Solar-Blind Deep Ultraviolet Photodetection. *Semicond. Sci. Technol.* **2017**, *32* (3), 03LT01.

(11) An, Y. H.; Guo, D. Y.; Li, S. Y.; Wu, Z. P.; Huang, Y. Q.; Li, P. G.; Li, L. H.; Tang, W. H. Influence of Oxygen Vacancies on the Photoresponse ofβ-Ga_2O_3/SiCn-ntype Heterojunctions. *J. Phys. D: Appl. Phys.* **2016**, *49* (28), 285111.

(12) Wang, X.; Chen, Z. W.; Guo, D. Y.; Zhang, X.; Wu, Z. P.; Li, P. G.; Tang, W. H. Optimizing the Performance of a β-Ga_2O_3 Solar-Blind UV Photodetector by Compromising between Photoabsorption and Electric Field Distribution. *Opt. Mater. Express* **2018**, *8* (9), 2918.

(13) Chen, H.; Liu, K.; Hu, L.; Al-Ghamdi, A. A.; Fang, X. New Concept Ultraviolet Photodetectors. *Mater. Today* **2015**, *18* (9), 493−502.

(14) Bo, R.; Nasiri, N.; Chen, H.; Caputo, D.; Fu, L.; Tricoli, A. Low-Voltage High-Performance UV Photodetectors: An Interplay

between Grain Boundaries and Debye Length. *ACS Appl. Mater. Interfaces* **2017**, *9* (3), 2606−2615.

(15) Chen, K.; He, C. R.; Guo, D. Y.; Wang, S. L.; Chen, Z. W.; Shen, J. Q.; Li, P. G.; Tang, W. H. Low-Voltage-Worked Photodetector Based on Cu_2O/GaOOH Shell-Core Heterojunction Nanorod Arrays. *J. Alloys Compd.* **2018**, *755*, 199−205.

(16) Lin, S.; Wang, H. Y.; Zhang, X. N.; Wang, D.; Zu, D.; Song, J. N.; Liu, Z. L.; Huang, Y.; Huang, K.; Tao, N.; Li, Z. W.; Bai, X. P.; Li, B.; Lei, M.; Yu, Z. F.; Wu, H. Direct Spray-Coating of Highly Robust and Transparent Ag Nanowires for Energy Saving Windows. *Nano Energy* **2019**, *62*, 111−116.

(17) Lin, S.; Wang, H. Y.; Wu, F.; Wang, Q. M.; Bai, X. P.; Zu, D.; Song, J. N.; Wang, D.; Liu, Z. L.; Li, Z. W.; Tao, N.; Huang, K.; Lei, M.; Li, B.; Wu, H. Room-Temperature Production of Silver-Nanofiber Film for Large-Area, Transparent and Flexible Surface Electromagnetic Interference Shielding. *Npj Flex. Electron* **2019**, *3* (1), 6.

(18) Wang, X. T.; Cui, Y.; Li, T.; Lei, M.; Li, J. B.; Wei, Z. M. Recent Advances in the Functional 2D Photonic and Optoelectronic Devices. *Adv. Opt. Mater.* **2019**, *7*, 1801274.

(19) Lin, S.; Bai, X. P.; Wang, H. Y.; Wang, H. L.; Song, J. N.; Huang, K.; Wang, C.; Wang, N.; Li, B.; Lei, M.; Wu, H. Roll-to-Roll Production of Transparent Silver Nanofiber Network Electrode for Flexible Electrochromic Smart Windows. *Adv. Mater.* **2017**, *29*, 1703238.

(20) Liu, Q.; Gong, M.; Cook, B.; Thapa, P.; Ewing, D.; Casper, M.; Stramel, A.; Wu, J. Oxygen Plasma Surface Activation of Electron-Depleted ZnO Nanoparticle Films for Performance-Enhanced Ultraviolet Photodetectors. *Phys. Status Solidi A* **2017**, *214* (11), 1700176.

(21) Ben Elkamel, I.; Hamdaoui, N.; Mezni, A.; Ajjel, R.; Beji, L. High Responsivity and 1/f Noise of an Ultraviolet Photodetector Based on Ni Doped ZnO Nanoparticles. *RSC Adv.* **2018**, *8* (56), 32333−32343.

(22) Li, L.; Jiang, H.; Han, X.; Zhan, Z.; Du, H.; Lu, W.; Li, Z.; Tao, Z.; Fan, Y. Optimizing Growth of ZnO Nanowire Networks for High-Performance UV Detection. *Ceram. Int.* **2017**, *43* (17), 15978−15985.

(23) Zhang, M.; Liu, Y.; Yang, M.; Zhang, W.; Zhou, J.; Zhang, Z.; Xie, E.; Pan, X.; Li, S. High Performance Self-Powered Ultraviolet Photodetectors Based on Electrospun Gallium Nitride Nanowires. *Appl. Surf. Sci.* **2018**, *452*, 43−48.

(24) Zhang, M.; Wang, Y.; Teng, F.; Chen, L.; Li, J.; Zhou, J.; Pan, X.; Xie, E. A Photoelectrochemical Type Self-Powered Ultraviolet Photodetector Based on GaN Porous Films. *Mater. Lett.* **2016**, *162*, 117−120.

(25) Zhou, H.; Gui, P.; Yang, L.; Ye, C.; Xue, M.; Mei, J.; Song, Z.; Wang, H. High Performance, Self-Powered Ultraviolet Photodetector Based on a ZnO Nanoarrays/GaN Structure with a CdS Insert Layer. *New J. Chem.* **2017**, *41* (12), 4901−4907.

(26) Zhang, Y.; Xu, J.; Shi, S.; Gao, Y.; Wang, C.; Zhang, X.; Yin, S.; Li, L. Development of Solution-Processed ZnO Nanorod Arrays Based Photodetectors and the Improvement of UV Photoresponse via AZO Seed Layers. *ACS Appl. Mater. Interfaces* **2016**, *8* (34), 22647−22657.

(27) Fu, Q. M.; He, D. C.; Yao, Z. C.; Peng, J. L.; Zhao, H. Y.; Tao, H.; Chen, Z.; Tu, Y. F.; Tian, Y.; Zhou, D.; Zheng, G.; Ma, Z. B. Self-Powered Ultraviolet Photodetector Based on ZnO Nanorod Arrays Decorated with Sea Anemone-Like CuO Nanostructures. *Mater. Lett.* **2018**, *222*, 74−77.

(28) Chen, D.; Wei, L.; Meng, L.; Wang, D.; Chen, Y.; Tian, Y.; Yan, S.; Mei, L.; Jiao, J. High-Performance Self-Powered UV Detector Based on SnO_2-TiO_2 Nanomace Arrays. *Nanoscale Res. Lett.* **2018**, *13* (1), 92.

(29) Ni, S.; Guo, F.; Wang, D.; Liu, G.; Xu, Z.; Kong, L.; Wang, J.; Jiao, S.; Zhang, Y.; Yu, Q.; Luo, J.; Wang, B.; Li, Z.; Zhang, C.; Zhao, L. Effect of MgO Surface Modification on the TiO_2 Nanowires Electrode for Self-Powered UV Photodetectors. *ACS Sustainable Chem. Eng.* **2018**, *6* (6), 7265−7272.

(30) He, T.; Zhao, Y.; Zhang, X.; Lin, W.; Fu, K.; Sun, C.; Shi, F.; Ding, X.; Yu, G.; Zhang, K.; Lu, S.; Zhang, X.; Zhang, B. Solar-Blind Ultraviolet Photodetector Based on Graphene/Vertical Ga_2O_3 Nanowire Array Heterojunction. *Nanophotonics* **2018**, *7* (9), 1557−1562.

(31) Guo, X. C.; Hao, N. H.; Guo, D. Y.; Wu, Z. P.; An, Y. H.; Chu, X. L.; Li, L. H.; Li, P. G.; Lei, M.; Tang, W. H. β-Ga_2O_3/*p*-Si Heterojunction Solar-Blind Ultraviolet Photodetector with Enhanced Photoelectric Responsivity. *J. Alloys Compd.* **2016**, *660*, 136−140.

(32) Li, P.; Shi, H.; Chen, K.; Guo, D.; Cui, W.; Zhi, Y.; Wang, S.; Wu, Z.; Chen, Z.; Tang, W. Construction of GaN/Ga_2O_3*p-n* Junction for an Extremely High Responsivity Self-Powered UV Photodetector. *J. Mater. Chem. C* **2017**, *5* (40), 10562−10570.

(33) Guo, D. Y.; Su, Y. L.; Shi, H. Z.; Li, P. G.; Zhao, N.; Ye, J. H.; Wang, S. L.; Liu, A. P.; Chen, Z. W.; Li, C. R.; Tang, W. H. Self-Powered Ultraviolet Photodetector with Super High Photoresponsivity (3.05 A/W) Based on the GaN/Sn:Ga_2O_3*pn* Junction. *ACS Nano* **2018**, *12*, 12827.

(34) Chen, X.; Liu, K.; Zhang, Z.; Wang, C.; Li, B.; Zhao, H.; Zhao, D.; Shen, D. Self-Powered Solar-Blind Photodetector with Fast Response Based on Au/β-Ga_2O_3 Nanowires Array Film Schottky Junction. *ACS Appl. Mater. Interfaces* **2016**, *8* (6), 4185−4191.

(35) Yang, C.; Liang, H.; Zhang, Z.; Xia, X.; Tao, P.; Chen, Y.; Zhang, H.; Shen, R.; Luo, Y.; Du, G. Self-Powered SBD Solar-Blind Photodetector Fabricated on the Single Crystal of β-Ga_2O_3. *RSC Adv.* **2018**, *8* (12), 6341−6345.

(36) Zhao, B.; Wang, F.; Chen, H.; Zheng, L.; Su, L.; Zhao, D.; Fang, X. An Ultrahigh Responsivity (9.7 mA W^{-1}) Self-Powered Solar-Blind Photodetector Based on Individual ZnO-Ga_2O_3 Heterostructures. *Adv. Funct. Mater.* **2017**, *27* (17), 1700264.

(37) Wang, Y.; Zhang, M.; Liu, X.; Sivalingam, Y.; Xie, E.; Han, W. Facile One-Pot Synthesis of Chain-Like Titanium Dioxide Nanostructure Arrays for Efficient Ultraviolet Sensing. *Appl. Surf. Sci.* **2018**, *449*, 239−243.

(38) He, C. R., Guo, D. Y., Chen, K., Wang, S. L., Shen, J. Q., Zhao, N., Liu, A. P., Zheng, Y. Y., Li, P. G.; Wu, Z. P., Li, C. R., Wu, F. M., Tang, W. H., α-Ga_2O_3 Nanorod Array-Cu_2O Microsphere *pn* Junctions for Self-Powered Spectrum-Distinguishable Photodetectors. *ACS Appl. Nano Mater.* **2019**, 24095.

(39) Lin, H. J.; Gao, H.; Gao, P. X. UV-Enhanced CO Sensing Using Ga_2O_3-Based Nanorod Arrays at Elevated Temperature. *Appl. Phys. Lett.* **2017**, *110* (4), 043101.

(40) Rao, R.; Rao, A. M.; Xu, B.; Dong, J.; Sharma, S.; Sunkara, M. K. Blueshifted Raman scattering and its correlation with the [110] growth direction in gallium oxide nanowires. *J. Appl. Phys.* **2005**, *98* (9), 094312.

(41) Machon, D.; McMillan, P. F.; Xu, B.; Dong, J. High-pressure study of the β-to-α transition in Ga_2O_3. *Phys. Rev. B: Condens. Matter Mater. Phys.* **2006**, *73* (9), 094125.

(42) Reddy, L. S.; Ko, Y. H.; Yu, J. S. Hydrothermal Synthesis and Photocatalytic Property of β-Ga_2O_3 Nanorods. *Nanoscale Res. Lett.* **2015**, *10* (1), 364.

(43) Wei, J.; Zang, Z.; Shi, F. Synthesis, Characterization and Growth Mechanism of β-Ga_2O_3 Nano- and Micrometer Particles by Catalyzed Chemical Vapor Deposition. *J. Mater. Sci.: Mater. Electron.* **2015**, *26* (10), 7731−7736.

(44) Quan, Y.; Fang, D.; Zhang, X.; Liu, S.; Huang, K. Synthesis and Characterization of Gallium Oxide Nanowires via a Hydrothermal Method. *Mater. Chem. Phys.* **2010**, *121* (1−2), 142−146.

(45) Wang, X.; Xu, Q.; Li, M.; Shen, S.; Wang, X.; Wang, Y.; Feng, Z.; Shi, J.; Han, H.; Li, C. Photocatalytic Overall Water Splitting Promoted by an α-β Phase Junction onGa_2O_3. *Angew. Chem., Int. Ed.* **2012**, *51* (52), 13089−13092.

(46) Hou, Y.; Zhang, J.; Ding, Z.; Wu, L. Synthesis, Characterization and Photocatalytic Activity of β-Ga_2O_3 Nanostructures. *Powder Technol.* **2010**, *203* (3), 440−446.

(47) Huang, W.; Xing, C.; Wang, Y.; Li, Z.; Wu, L.; Ma, D.; Dai, X.; Xiang, Y.; Li, J.; Fan, D.; Zhang, H. Facile Fabrication and Characterization of Two-Dimensional Bismuth (III) Sulfide Nanosheets for High-Performance Photodetector Applications under Ambient Conditions. *Nanoscale* **2018**, *10* (5), 2404−2412.

(48) Lee, H.; Heo, K.; Park, J.; Park, Y.; Noh, S.; Kim, K. S.; Lee, C.; Hong, B. H.; Jian, J.; Hong, S. Graphene-Nanowire Hybrid Structures for High-Performance Photoconductive Devices. *J. Mater. Chem.* **2012**, *22* (17), 8372−8376.

(49) Guo, D. Y.; Wang, J. B.; Cui, C.; Li, P. G.; Zhong, X. L.; Wang, F.; Yuan, S. G.; Zhang, K. D.; Zhou, Y. C. ZnO@TiO_2 Core-Shell Nanorod Arrays with Enhanced Photoelectrochemical Performance. *Sol. Energy* **2013**, *95*, 237−245.

(50) Masudy-Panah, S.; Siavash Moakhar, R.; Chua, C. S.; Tan, H. R.; Wong, T. I.; Chi, D.; Dalapati, G. K. Nanocrystal Engineering of Sputter-Grown CuO Photocathode for Visible-Light-Driven Electrochemical Water Splitting. *ACS Appl. Mater. Interfaces* **2016**, *8* (2), 1206−1213.

(51) Yang, Y.; Han, J.; Ning, X.; Cao, W.; Xu, W.; Guo, L. Controllable Morphology and Conductivity of Electrodeposited Cu_2O Thin Film: Effect of Surfactants. *ACS Appl. Mater. Interfaces* **2014**, *6* (24), 22534−22543.

(52) Yu, L.; Li, G.; Zhang, X.; Ba, X.; Shi, G.; Li, Y.; Wong, P. K.; Yu, J. C.; Yu, Y. Enhanced Activity and Stability of Carbon-Decorated Cuprous Oxide Mesoporous Nanorods for CO_2 Reduction in Artificial Photosynthesis. *ACS Catal.* **2016**, *6* (10), 6444−6454.

(53) Yuan, W.; Yuan, J.; Xie, J.; Li, C. M. Polymer-Mediated Self-Assembly of TiO_2@Cu_2O Core-Shell Nanowire Array for Highly Efficient Photoelectrochemical Water Oxidation. *ACS Appl. Mater. Interfaces* **2016**, *8* (9), 6082−6092.

(54) Majumder, T.; Hmar, J. J. L.; Debnath, K.; Gogurla, N.; Roy, J. N.; Ray, S. K.; Mondal, S. P. Photoelectrochemical and Photosensing Behaviors of Hydrothermally Grown ZnO Nanorods. *J. Appl. Phys.* **2014**, *116* (3), 034311.

(55) Cao, C.; Hu, C.; Wang, X.; Wang, S.; Tian, Y.; Zhang, H. UV Sensor Based on TiO_2 Nanorod Arrays on FTO Thin Film. *Sens. Actuators, B* **2011**, *156* (1), 114−119.

(56) Bai, Z.; Liu, J.; Liu, F.; Zhang, Y. Enhanced Photoresponse Performance of Self-Powered UV-Visible Photodetectors Based on ZnO/Cu_2O/Electrolyte Heterojunctions via Graphene Incorporation. *J. Alloys Compd.* **2017**, *726*, 803−809.

(57) Li, Q. H.; Wei, L.; Xie, Y. R.; Zhang, K.; Liu, L.; Zhu, D. P.; Jiao, J.; Chen, Y. X.; Yan, S. S.; Liu, G. L.; Mei, L. M. ZnO Nanoneedle/H_2O Solid-Liquid Heterojunctionbased Self-Powered Ultraviolet Detector. *Nanoscale Res. Lett.* **2013**, *8* (415), 1−7.

(58) Xie, Y. R.; Wei, L.; Wei, G. D.; Li, Q. H.; Wang, D.; Chen, Y. X.; Yan, S. S.; Liu, G. L.; Mei, L. M.; Jiao, J. A Self-Powered UV Photodetector Based on TiO_2 Nanorod Arrays. *Nanoscale Res. Lett.* **2013**, *8* (188), 1−6.

(59) Zhang, J. H.; Jiao, S. J.; Wang, D. B.; Ni, S. M.; Gao, S. Y.; Wang, J. Z. Solar-blind ultraviolet photodetection of an α-Ga_2O_3 nanorod array based on photoelectrochemical self-powered detectors with a simple, newly-designed structure. *J. Mater. Chem. C* **2019**, *7* (23), 6867−6871.

DOI: 10.1021/acsanm.9b00992
ACS Appl. Nano Mater. 2019, 2, 6169−6177